

Analysis of period and visibility of dual phase grating interferometer

Jun Yang(杨君), Jian-Heng Huang(黄建衡), Yao-Hu Lei(雷耀虎), Jing-Biao Zheng(郑景标), Yu-Zheng Shan(单雨征), Da-Yu Guo(郭大育), and Jin-Chuan Guo(郭金川)

Citation: Chin. Phys. B, 2022, 31 (**5**): 058701. DOI: 10.1088/1674-1056/ac3a60
Journal homepage: http://cpb.iphy.ac.cn; http://iopscience.iop.org/cpb

What follows is a list of articles you may be interested in

Quantitative coherence analysis of dual phase grating x-ray interferometry with source grating

Zhi-Li Wang(王志立), Rui-Cheng Zhou(周瑞成), Li-Ming Zhao(赵立明), Kun Ren(任坤), Wen Xu(徐文), Bo Liu(刘波), and Heng Chen(陈恒)

Chin. Phys. B, 2021, 30 (**2**): 028702. DOI: 10.1088/1674-1056/abb7fd

Single-shot grating-based x-ray differential phase contrast imaging with a modified analyzer grating

Chen-Xi Wei(卫晨希), Zhao Wu(吴朝), Faiz Wali, Wen-Bin Wei(魏文彬), Yuan Bao(鲍园), Rong-Hui Luo(骆荣辉), Lei Wang(王磊), Gang Liu(刘刚), Yang-Chao Tian(田扬超)

Chin. Phys. B, 2017, 26 (**10**): 108701. DOI: 10.1088/1674-1056/26/10/108701

Shifting curves based on the detector integration effect for x-ray phase contrast imaging

Jun Yang(杨君), Jin-Chuan Guo(郭金川), Yao-Hu Lei(雷耀虎), Ming-Hao Yi(易明皓), Li Chen(陈力)

Chin. Phys. B, 2017, 26 (**2**): 028701. DOI: 10.1088/1674-1056/26/2/028701

Elemental x-ray imaging using Zernike phase contrast

Qi-Gang Shao(邵其刚), Jian Chen(陈健), Faiz Wali, Yuan Bao(鲍园), Zhi-Li Wang(王志立), Pei-Ping Zhu(朱佩平), Yang-Chao Tian(田扬超), Kun Gao(高昆)

Chin. Phys. B, 2016, 25 (**10**): 108702. DOI: 10.1088/1674-1056/25/10/108702

Simple phase extraction in x-ray differential phase contrast imaging

Xin Liu(刘鑫), Jin-Chuan Guo(郭金川), Yao-Hu Lei(雷耀虎), Ji Li(李冀), Han-Ben Niu(牛憨笨)

Chin. Phys. B, 2016, 25 (**2**): 028704. DOI: 10.1088/1674-1056/25/2/028704

Analysis of period and visibility of dual phase grating interferometer

Jun Yang(杨君), Jian-Heng Huang(黄建衡), Yao-Hu Lei(雷耀虎), Jing-Biao Zheng(郑景标), Yu-Zheng Shan(单雨征), Da-Yu Guo(郭大育), and Jin-Chuan Guo(郭金川)†

Key Laboratory of Optoelectronic Devices and Systems of Ministry of Education and Guangdong Province, College of Physics and Optoelectronic Engineering, Shenzhen University, Shenzhen 518060, *China*

(Received 17 September 2021; revised manuscript received 1 November 2021; accepted manuscript online 17 November 2021)

Dual phase grating interferometer may simultaneously achieve large field of view and high x-ray dose efficiency. Here, we develop a simple theoretical method to better understand the imaging process of the dual phase grating interferometer. The derivation process of fringe period and the optimal visibility conditions of the dual phase grating interferometer are given in detail. Then, we theoretically prove that the fringe period and optimal visibility conditions of the dual phase grating interferometer include that of the Talbot interferometer. By comparing our experimental results with those of other researchers, we find that when the positions of phase gratings are far away from the positions where the fringe visibility is optimal, the fringe period of the dual π-phase grating interferometer is twice the theoretical results under the illumination of polychromatic x-ray. This conclusion may explain the contradictory research results of dual phase grating interferometer among different researchers.

Keywords: phase contrast, grating interferometer, fringe period, fringe visibility

PACS: 87.59.–e, 87.64.mh, 07.60.Ly, 87.57.C– **DOI:** 10.1088/1674-1056/ac3a60

1. Introduction

X-ray phase-contrast images and dark-field images obtained by a Talbot–Lau interferometer have potential applications in diagnosis of rheumatoid arthritis, microcalcifications in breast and lung diseases.[1–14] However, the Talbot–Lau interferometer is restricted by the small field of view in clinic applications. It is a great challenge to fabricate the analyzer grating over a large area and high aspect ratio. The inverse geometry Talbot–Lau interferometer,[15] which interchanges the position of the x-ray source and the detector, does not need any analyzer grating. However, its high system magnification will also reduce the field of view. Miao *et al.*[16] used a dual phase grating interferometer to produce fringes with large periods. The dual phase grating interferometer does not use the analyzer grating, and it may provide a larger field of view and higher x-ray dose efficiency. Kagias *et al.*[17] connected dual Talbot interferometers together for dark-field imaging. The idea of virtual structure source proposed in their paper is very instructive for understanding the imaging process. Lei *et al.*[18] realized a dual Talbot–Lau interferometer in which the addition of source grating overcame the limitation of flux of micro-focal spot source. Ge *et al.*[7] proposed that under the optical reversibility principle, the phase gratings in the dual phase grating interferometer could be treated as thin lens. However, the aforementioned theoretical calculations were too complicated.[7,16,19] What's more, the theoretical and experimental results given by different researchers were inconsistent. For example, the fringe period given by Miao *et al.*[16] was twice as long as the fringe period given by Ge *et al.*[7] In this paper, we will work to simplify the theoretical analysis and explain these different theoretical and experimental results.

2. Theoretical analysis

2.1. Dual phase grating interferometer

Considering Fig. 1, let us assume that a point source with a wavelength λ is in the plane x_0oy_0, the first phase grating G1 with period p_1 is in the plane x_1oy_1, the second phase grating G2 with period p_2 is in the plane x_2oy_2, and the detector is in the plane x_3oy_3. The distance from the source to the first phase grating, the first phase grating to the second phase grating, and the second phase grating to the detector are z_1, z_2 and z_3, respectively.

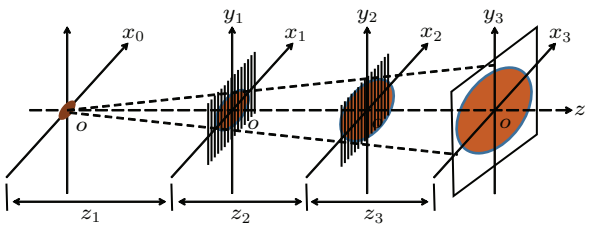


Fig. 1. Setup of the dual phase grating interferometer.

According to the Fourier series theory, the complex amplitude distributions of the first phase grating G1 and the second phase grating G2 may be expressed as

$$T_1(x_1) = \sum_{n=-\infty}^{\infty} a_n \exp\left(\mathrm{j}2\pi \frac{n}{p_1} x_1\right), \tag{1}$$

$$T_2(x_2) = \sum_{n=-\infty}^{\infty} b_m \exp\left(\mathrm{j}2\pi \frac{m}{p_2} x_2\right), \tag{2}$$

†Corresponding author. E-mail: jcguo@szu.edu.cn

© 2022 Chinese Physical Society and IOP Publishing Ltd

where a_n and b_m are Fourier coefficients, and their expressions are as follows:

$$a_n = \begin{cases} \frac{1}{2}\left(1+\mathrm{e}^{\mathrm{j}\phi}\right), & n=0, \\ \left(\mathrm{e}^{\mathrm{j}\phi}-1\right)\dfrac{\sin\left(\frac{n\pi}{2}\right)}{n\pi}, & n\neq 0, \end{cases} \tag{3}$$

$$b_m = \begin{cases} \frac{1}{2}\left(1+\mathrm{e}^{\mathrm{j}\phi}\right), & m=0, \\ \left(\mathrm{e}^{\mathrm{j}\phi}-1\right)\dfrac{\sin\left(\frac{m\pi}{2}\right)}{m\pi}, & m\neq 0, \end{cases} \tag{4}$$

where φ is the phase shift of the phase grating, and the duty cycle of the two phase gratings is 50%. The wave field on the front surface of the plane x_1oy_1 is given by

$$U_1(x_1) = \frac{A_1}{z_1}\mathrm{e}^{\mathrm{j}kz_1}\exp\left(\frac{\mathrm{j}k}{2z_1}x_1^2\right), \tag{5}$$

where $k = 2\pi/\lambda$, A_1 is the amplitude of wave fields at unit distance from the source, and the disturbance of wave fields on the back surface of the plane x_1oy_1 may be expressed as

$$U_2(x_1) = U_1(x_1)\,T_1(x_1). \tag{6}$$

After Fresnel diffraction, the distribution of wave fields on the front surface of the plane x_2oy_2 is as follows:

$$U_3(x_2) = \frac{1}{\sqrt{\mathrm{j}\lambda}}\int_{x_1=-\infty}^{\infty} U_2(x_1)\frac{\mathrm{e}^{\mathrm{j}kr_1}}{z_2}\mathrm{d}x_1, \tag{7}$$

where r_1 is the distance from the point on the plane x_1oy_1 to the point on the plane x_2oy_2. Substituting Eqs. (1), (5), (6) in Eq. (7) yields

$$\begin{aligned} U_3(x_2) = {} & \frac{1}{\sqrt{\mathrm{j}\lambda}}\int_{x_1=-\infty}^{\infty}\frac{A_1}{z_1}\mathrm{e}^{\mathrm{j}kz_1}\exp\left(\frac{\mathrm{j}k}{2z_1}x_1^2\right)\frac{\mathrm{e}^{\mathrm{j}kz_2}}{z_2} \\ & \times\exp\left[\frac{\mathrm{j}k}{2z_2}(x_2-x_1)^2\right] \\ & \times\sum_{n=-\infty}^{\infty}a_n\exp\left(\mathrm{j}2\pi\frac{n}{p_1}x_1\right)\mathrm{d}x_1. \end{aligned} \tag{8}$$

Equation (8) may be simplified to

$$U_3(x_2) = A_3\sum_{n=-\infty}^{\infty}a_n\exp\left(-\mathrm{j}\pi pn^2\right)\exp\left(\mathrm{j}2\pi n\frac{x_2}{M_1p_1}\right), \tag{9}$$

where A_3 is a constant coefficient, p is the Talbot order, and M_1 is the magnification of the first grating, namely,

$$A_3 = \frac{A_1\exp\left[\mathrm{j}k(z_1+z_2)\right]}{\sqrt{z_1z_2(z_1+z_2)}}\exp\left[\frac{\mathrm{j}kx_2^2}{2(z_1+z_2)}\right], \tag{10}$$

$$p = \frac{\lambda z_2}{M_1p_1^2}, \tag{11}$$

$$M_1 = \frac{z_1+z_2}{z_1}. \tag{12}$$

The wave field on the back surface of the plane x_2oy_2 may be written as

$$U_4(x_2) = U_3(x_2)\,T_2(x_2). \tag{13}$$

After Fresnel diffraction, the wave field over the plane x_3oy_3 is described as

$$U_5(x_3) = \frac{\exp(\mathrm{j}kz_3)}{\sqrt{\mathrm{j}\lambda}z_3}\int_{x_2=-\infty}^{\infty}\exp\left[\frac{\mathrm{j}k}{2z_3}(x_3-x_2)^2\right]U_4(x_2)\,\mathrm{d}x_2. \tag{14}$$

Substituting Eqs. (2), (9) and (13) into Eq. (14), we arrive at the following simplified expression:

$$\begin{aligned} U_5(x_3) = {} & A_5\sum_{n=-\infty}^{\infty}\sum_{m=-\infty}^{\infty}a_nb_m\exp\left(-\mathrm{j}\pi pn^2\right) \\ & \times\exp\left[-\mathrm{j}\pi\frac{\lambda z_3}{M_2}\left(\frac{n}{M_1p_1}+\frac{m}{p_2}\right)^2\right] \\ & \times\exp\left[\mathrm{j}2\pi\frac{x_3}{M_2}\left(\frac{n}{M_1p_1}+\frac{m}{p_2}\right)\right], \end{aligned} \tag{15}$$

where $M_2 = \frac{z_1+z_2+z_3}{z_1+z_2}$, A_5 is a constant coefficient given by

$$A_5 = \frac{A_1\exp\left[\mathrm{j}k(z_1+z_2+z_3)\right]}{\sqrt{z_1z_2z_3(z_1+z_2+z_3)}}\exp\left[\frac{\mathrm{j}kx_3^2}{2(z_1+z_2+z_3)}\right]. \tag{16}$$

Equation (15) is the general expression of wave fields of dual phase grating interferometer under a point source illumination.[7]

2.2. Relationship between the dual phase grating interferometer and the Talbot interferometer

Since detectors only receive the intensity signals, the phase factor in Eq. (16) may be ignored and we obtain

$$\begin{aligned} U_6(x_3) = {} & \sum_{n=-\infty}^{\infty}\sum_{m=-\infty}^{\infty}a_nb_m\exp\left(-\mathrm{j}\pi pn^2\right) \\ & \times\exp\left[-\mathrm{j}\pi\frac{\lambda z_3}{M_2}\left(\frac{n}{M_1p_1}+\frac{m}{p_2}\right)^2\right] \\ & \times\exp\left[\mathrm{j}2\pi\frac{x_3}{M_2}\left(\frac{n}{M_1p_1}+\frac{m}{p_2}\right)\right]. \end{aligned} \tag{17}$$

Case 1 Set the phase shift of the first phase grating to zero. This turns it into a phase plate, which is equivalent to the absence of the first phase grating. Then,

$$a_n = \begin{cases} 1, & n=0, \\ 0, & n\neq 0. \end{cases} \tag{18}$$

At this point, Eq. (17) transforms to

$$U_6(x_3) = \sum_{m=-\infty}^{\infty}b_m\exp\left[-\mathrm{j}\pi\frac{\lambda z_3}{M_2}\frac{m^2}{p_2^2}\right]\exp\left[\mathrm{j}2\pi\frac{x_3}{M_2}\frac{m}{p_2}\right]. \tag{19}$$

Since Eqs. (19) and (9) are identical except for the phase factor, Eq. (19) may be regarded as the imaging formula of the Talbot interferometer.

Case 2 Set the phase shift of the second phase grating to zero. This makes the second phase grating a phase plate, which is equivalent to the absence of the second phase grating. Then,

$$b_m = \begin{cases} 1, & n=0, \\ 0, & n\neq 0, \end{cases} \tag{20}$$

$$
\begin{aligned}
U_6(x_3) &= \sum_{n=-\infty}^{\infty} a_n \exp\left(-\mathrm{j}\pi p n^2\right) \exp\left(-\mathrm{j}\pi \frac{\lambda z_3}{M_2} \frac{n^2}{M_1^2 p_1^2}\right) \exp\left(\mathrm{j}2\pi \frac{x_3}{M_2} \frac{n}{M_1 p_1}\right) \\
&= \sum_{n=-\infty}^{\infty} a_n \exp\left[-\mathrm{j}\pi \left(\frac{\lambda z_2}{M_1 p_1^2} + \frac{\lambda z_3}{M_2 M_1^2 p_1^2}\right) n^2\right] \exp\left(\mathrm{j}2\pi \frac{x_3 n}{M_1 M_2 p_1}\right) \\
&= \sum_{n=-\infty}^{\infty} a_n \exp\left[-\mathrm{j}\pi\lambda \left(\frac{z_1 z_2}{z_1+z_2} + \frac{z_3 z_1^2}{(z_1+z_2+z_3)(z_1+z_2)}\right) \frac{n^2}{p_1^2}\right] \exp\left(\mathrm{j}2\pi \frac{x_3 n}{M_1 M_2 p_1}\right) \\
&= \sum_{n=-\infty}^{\infty} a_n \exp\left(-\mathrm{j}\pi\lambda \frac{z_2+z_3}{M_3} \frac{n^2}{p_1^2}\right) \exp\left(\mathrm{j}2\pi \frac{x_3 n}{M_3 p_1}\right), \qquad (21)
\end{aligned}
$$

where $M_3 = M_1 M_2 = \frac{z_1+z_2+z_3}{z_1}$. We find that formula (9) is quite similar to formula (21), which also degenerates to the case of the Talbot interferometer. Hence, it may be concluded that the Talbot interferometer is a special case of dual phase grating interferometer.

2.3. Fringe periods of dual phase grating interferometer

Next, we will derive the fringe periods of the dual phase grating interferometer from Eq. (17). If we let

$$
C_{n,m} = a_n b_m \exp\left(-\mathrm{j}\pi p n^2\right) \exp\left[-\mathrm{j}\pi \frac{\lambda z_3}{M_2} \left(\frac{n}{M_1 p_1} + \frac{m}{p_2}\right)^2\right] \times \exp\left[\mathrm{j}2\pi \frac{x_3}{M_2} \left(\frac{n}{M_1 p_1} + \frac{m}{p_2}\right)\right], \qquad (22)
$$

then we have

$$
U_6(x_3) = \sum_{n=-\infty}^{\infty} \sum_{m=-\infty}^{\infty} C_{n,m}. \qquad (23)
$$

The intensity distribution may be expressed as

$$
\begin{aligned}
I &= \sum_{n=-\infty}^{\infty} \sum_{m=-\infty}^{\infty} C_{n,m} \cdot \sum_{s=-\infty}^{\infty} \sum_{t=-\infty}^{\infty} C_{s,t}^* \\
&= \sum_{n=-\infty}^{\infty} \sum_{m=-\infty}^{\infty} \sum_{s=-\infty}^{\infty} \sum_{t=-\infty}^{\infty} C_{n,m} C_{s,t}^*, \qquad (24)
\end{aligned}
$$

$$
C_{s,t}^* = a_s^* b_t^* \exp\left(\mathrm{j}\pi p s^2\right) \exp\left[\mathrm{j}\pi \frac{\lambda z_3}{M_2} \left(\frac{s}{M_1 p_1} + \frac{t}{p_2}\right)^2\right] \exp\left[-\mathrm{j}2\pi \frac{x_3}{M_2} \left(\frac{s}{M_1 p_1} + \frac{t}{p_2}\right)\right], \qquad (25)
$$

$$
C_{n,m} C_{s,t}^* = a_n b_m a_s^* b_t^* \exp\left[\mathrm{j}\pi p \left(s^2 - n^2\right)\right] \exp\left[\mathrm{j}\pi \frac{\lambda z_3}{M_2} \left(\frac{s^2-n^2}{M_1^2 p_1^2} + \frac{t^2-m^2}{p_2^2} + \frac{2st-2mn}{M_1 p_1 p_2}\right)\right] \exp\left[\mathrm{j}2\pi \frac{x_3}{M_2} \left(\frac{n-s}{M_1 p_1} + \frac{m-t}{p_2}\right)\right]. \qquad (26)
$$

The conjugate term of Eq. (26) is

$$
\begin{aligned}
C_{s,t} C_{n,m}^* &= a_s b_t a_n^* b_m^* \exp\left[-\mathrm{j}\pi p \left(s^2 - n^2\right)\right] \exp\left[-\mathrm{j}\pi \frac{\lambda z_3}{M_2} \left(\frac{s^2-n^2}{M_1^2 p_1^2} + \frac{t^2-m^2}{p_2^2} + \frac{2st-2mn}{M_1 p_1 p_2}\right)\right] \\
&\quad \times \exp\left[-\mathrm{j}2\pi \frac{x_3}{M_2} \left(\frac{n-s}{M_1 p_1} + \frac{m-t}{p_2}\right)\right]. \qquad (27)
\end{aligned}
$$

Adding Eqs. (26) and (27) yields

$$
\begin{aligned}
C_{n,m} C_{s,t}^* + C_{s,t} C_{n,m}^* &= 2\left|a_n b_m a_s^* b_t^*\right| \cos\left[2\pi \frac{x_3}{M_2} \left(\frac{n-s}{M_1 p_1} + \frac{m-t}{p_2}\right) + \pi \frac{\lambda z_3}{M_2} \left(\frac{s^2-n^2}{M_1^2 p_1^2} + \frac{t^2-m^2}{p_2^2} + \frac{2st-2mn}{M_1 p_1 p_2}\right)\right. \\
&\quad \left. + \pi p \left(s^2 - n^2\right) + \varphi\right], \qquad (28)
\end{aligned}
$$

where φ is the argument of $a_n b_m a_s^* b_t^*$. We have

$$
a_n b_m a_s^* b_t^* = \frac{\left[\exp(\mathrm{j}\phi) - 1\right]^2 \left[\exp(-\mathrm{j}\phi) - 1\right]^2}{nmst\pi^4} \sin\left(\frac{n\pi}{2}\right) \sin\left(\frac{m\pi}{2}\right) \sin\left(\frac{s\pi}{2}\right) \sin\left(\frac{t\pi}{2}\right). \qquad (29)
$$

Next, we will consider the cases when two gratings are π and $\pi/2$ phase gratings.

Case 1 Both phase gratings are π-phase gratings.

In this case, Eq. (29) may be expressed as

$$
a_n b_m a_s^* b_t^* = \frac{16}{nmst\pi^4} \sin\left(\frac{n\pi}{2}\right) \sin\left(\frac{m\pi}{2}\right) \sin\left(\frac{s\pi}{2}\right) \sin\left(\frac{t\pi}{2}\right). \qquad (30)
$$

Next, we consider the maximum amplitude terms in Eq. (28) except for the constant terms. Since we use phase gratings with a duty cycle of 50%, the sum coefficients n, m, s, t cannot be even. Therefore, there are six non-constant terms with the largest amplitude in Eq. (28),

$$C_{-1,-1}C^*_{-1,1}+C_{-1,1}C^*_{-1,-1} = \frac{32}{\pi^4}\cos\left(2\pi\frac{x_3}{M_2}\frac{-2}{p_2}+\frac{\pi\lambda z_3}{M_2}\frac{-4}{M_1p_1p_2}\right), \tag{31}$$

$$C_{-1,-1}C^*_{1,-1}+C_{1,-1}C^*_{-1,-1} = \frac{32}{\pi^4}\cos\left(2\pi\frac{x_3}{M_2}\frac{-2}{M_1p_1}+\frac{\pi\lambda z_3}{M_2}\frac{-4}{M_1p_1p_2}\right), \tag{32}$$

$$C_{-1,-1}C^*_{1,1}+C_{1,1}C^*_{-1,-1} = \frac{32}{\pi^4}\cos\left[2\pi\frac{x_3}{M_2}\left(\frac{-2}{M_1p_1}+\frac{-2}{p_2}\right)\right], \tag{33}$$

$$C_{-1,1}C^*_{1,-1}+C_{1,-1}C^*_{-1,1} = \frac{32}{\pi^4}\cos\left[2\pi\frac{x_3}{M_2}\left(\frac{-2}{M_1p_1}+\frac{2}{p_2}\right)\right], \tag{34}$$

$$C_{-1,1}C^*_{1,1}+C_{1,1}C^*_{-1,1} = \frac{32}{\pi^4}\cos\left(2\pi\frac{x_3}{M_2}\frac{-2}{M_1p_1}+\frac{\pi\lambda z_3}{M_2}\frac{4}{M_1p_1p_2}\right), \tag{35}$$

$$C_{1,-1}C^*_{1,1}+C_{1,1}C^*_{1,-1} = \frac{34}{\pi^4}\cos\left(2\pi\frac{x_3}{M_2}\frac{-2}{p_2}+\frac{\pi\lambda z_3}{M_2}\frac{4}{M_1p_1p_2}\right). \tag{36}$$

From Eqs. (31)–(36), we may see that there are four fringe frequencies, i.e., the fringe frequencies of the first phase grating in the imaging plane: $\frac{2}{M_1M_2p_1}$; the fringe frequencies of the second phase grating in the imaging plane: $\frac{2}{M_2p_2}$; the sum frequencies of two phase grating imaging fringes: $\frac{2}{M_1M_2p_1}+\frac{2}{M_2p_2}$; and the difference frequencies of two phase grating imaging fringes: $\left|\frac{2}{M_1M_2p_1}-\frac{2}{M_2p_2}\right|$.

Now we consider the case in which two phase gratings with very small period produce fringes with very large period. Under this condition, the difference frequency of two phase gratings imaging fringes will be much smaller than the other three frequencies. When the fringes of various frequencies are overlapped together, due to the focus size of the x-ray source and the integration effect of detector pixels, a low-pass filtering effect may be observed. When the system parameters satisfy certain conditions (discussed later), the difference frequency will be strengthened and other frequencies will be further suppressed. Hence, the final fringe frequency will be the difference frequency of two phase gratings:

$$f_3 = \left|\frac{2}{M_1M_2p_1}-\frac{2}{M_2p_2}\right|. \tag{37}$$

Equation (37) may be transformed into fringe period as follows:

$$p_3 = \frac{1}{2}\left|\frac{Lp_1p_2}{z_1p_2-(z_1+z_2)p_1}\right|, \tag{38}$$

where $L=z_1+z_2+z_3$. When $p_1\to\infty$ or $p_2\to\infty$, Eq. (38) will transform into the fringe period of the Talbot interferometer. If the dual phase grating interferometer is symmetrical, we will have

$$p_1 = p_2, \tag{39}$$

$$z_1 = z_3. \tag{40}$$

Then Eq. (38) may be transformed into

$$p_3 = \frac{1}{2}\frac{L}{z_2}p_1. \tag{41}$$

Note that Eq. (41) is the same as Aimin's results.[19] So far, we have obtained fringe period (Eq. (38)) for the dual phase grating interferometer.

Case 2 Both phase gratings are $\pi/2$-phase gratings.

The analysis method is similar to case 1 and the fringe period is as follows:

$$p_3 = \left|\frac{Lp_1p_2}{z_1p_2-(z_1+z_2)p_1}\right|. \tag{42}$$

2.4. Optimal visibility conditions of the dual phase grating interferometer

For the analysis of the optimal visibility conditions of the dual phase grating interferometer, two cases of dual phase grating of π and $\pi/2$ are discussed.

Case 1 Dual π-phase grating interferometer.

In order to maximize the fringes visibility in the dual π-phase grating interferometer, it is necessary to make the amplitudes different, but the phases of the fringes with the same frequency as $\left|\frac{2}{M_1M_2p_1}-\frac{2}{M_2p_2}\right|$ are the same. In practical analysis, we should focus on the relationship between the phases of the first few fringes whose amplitude is large and whose frequency is $\left|\frac{2}{M_1M_2p_1}-\frac{2}{M_2p_2}\right|$. The fringes with a frequency of $\left|\frac{2}{M_1M_2p_1}-\frac{2}{M_2p_2}\right|$ with the second largest amplitude have the following four items:

$$C_{-1,3}C^*_{1,1}+C_{1,1}C^*_{-1,3} = \frac{-32}{3\pi^4}\cos\left[2\pi\frac{x_3}{M_2}\left(\frac{-2}{M_1p_1}+\frac{2}{p_2}\right)+\frac{\pi\lambda z_3}{M_2}\left(\frac{-8}{p_2^2}+\frac{8}{M_1p_1p_2}\right)\right], \tag{43}$$

$$C_{-1,-1}C^*_{1,-3}+C_{1,-3}C^*_{-1,-1} = \frac{-32}{3\pi^4}\cos\left[2\pi\frac{x_3}{M_2}\left(\frac{-2}{M_1p_1}+\frac{2}{p_2}\right)+\frac{\pi\lambda z_3}{M_2}\left(\frac{8}{p_2^2}-\frac{8}{M_1p_1p_2}\right)\right], \tag{44}$$

$$C_{-3,1}C^*_{-1,-1}+C_{-1,-1}C^*_{-3,1}=\frac{-32}{3\pi^4}\cos\left[2\pi\frac{x_3}{M_2}\left(\frac{-2}{M_1p_1}+\frac{2}{p_2}\right)+\frac{\pi\lambda z_3}{M_2}\left(\frac{-8}{M_1^2p_1^2}+\frac{8}{M_1p_1p_2}\right)-8p\pi\right], \tag{45}$$

$$C_{1,1}C^*_{3,-1}+C_{3,-1}C^*_{1,1}=\frac{-32}{3\pi^4}\cos\left[2\pi\frac{x_3}{M_2}\left(\frac{-2}{M_1p_1}+\frac{2}{p_2}\right)+\frac{\pi\lambda z_3}{M_2}\left(\frac{8}{M_1^2p_1^2}-\frac{8}{M_1p_1p_2}\right)+8p\pi\right]. \tag{46}$$

Comparing Eqs. (34) and (43)–(46), it may be found that there is a negative sign before Eqs. (43)–(46), so it is necessary to add a π phase or a $-\pi$ phase in Eqs. (43)–(46). It may also be observed that the initial phases of Eqs. (43) and (44) are opposite to each other, as is the case for Eqs. (45) and (46). The initial phase of formula (34) is zero. Therefore, if the fringes represented by Eqs. (43)–(46) and (34) are mutually reinforcing, they need to be in the same phase. Then, the following relations must be satisfied:

$$\begin{cases}\dfrac{\pi\lambda z_3}{M_2}\left(\dfrac{8}{p_2^2}-\dfrac{8}{M_1p_1p_2}\right)+\pi=2h_1\pi,\\ \dfrac{\pi\lambda z_3}{M_2}\left(\dfrac{8}{M_1^2p_1^2}-\dfrac{8}{M_1p_1p_2}\right)+\pi+8\pi p=2h_2\pi,\end{cases} \tag{47}$$

where h_1 and h_2 are integers. Equation (47) may be simplified to

$$\begin{cases}\dfrac{\lambda z_3}{M_2}\left(\dfrac{1}{p_2^2}-\dfrac{1}{M_1p_1p_2}\right)=\dfrac{2h_1-1}{8},\\ \dfrac{\lambda z_3}{M_2}\left(\dfrac{1}{M_1^2p_1^2}-\dfrac{1}{M_1p_1p_2}\right)+p=\dfrac{2h_2-1}{8}.\end{cases} \tag{48}$$

Here, Eqs. (48) are the optimal visibility conditions for dual π-phase grating interferometer. When $p_1\to\infty$ or $p_2\to\infty$, Eqs. (48) will transform into the optimal visibility condition of the Talbot interferometer. Next, we ascertain whether the third strongest fringe with the same frequency as Eq. (34) may satisfy the condition represented by Eq. (48).

$$C_{-3,3}C^*_{-1,1}+C_{-1,1}C^*_{-3,3}=\frac{32}{9\pi^4}\cos\left[2\pi\frac{x_3}{M_2}\left(\frac{-2}{M_1p_1}+\frac{2}{p_2}\right)+\frac{\pi\lambda z_3}{M_2}\left(\frac{-8}{M_1^2p_1^2}+\frac{-8}{p_2^2}+\frac{16}{M_1p_1p_2}\right)-8\pi p\right], \tag{49}$$

$$C_{-3,-1}C^*_{-1,-3}+C_{-1,-3}C^*_{-3,-1}=\frac{32}{9\pi^4}\cos\left[2\pi\frac{x_3}{M_2}\left(\frac{-2}{M_1p_1}+\frac{2}{p_2}\right)+\frac{\pi\lambda z_3}{M_2}\left(\frac{-8}{M_1^2p_1^2}+\frac{8}{p_2^2}\right)-8\pi p\right], \tag{50}$$

$$C_{1,3}C^*_{3,1}+C_{3,1}C^*_{1,3}=\frac{32}{9\pi^4}\cos\left[2\pi\frac{x_3}{M_2}\left(\frac{-2}{M_1p_1}+\frac{2}{p_2}\right)+\frac{\pi\lambda z_3}{M_2}\left(\frac{8}{M_1^2p_1^2}-\frac{8}{p_2^2}\right)+8\pi p\right], \tag{51}$$

$$C_{1,-1}C^*_{3,-3}+C_{3,-3}C^*_{1,-1}=\frac{32}{9\pi^4}\cos\left[2\pi\frac{x_3}{M_2}\left(\frac{-2}{M_1p_1}+\frac{2}{p_2}\right)+\frac{\pi\lambda z_3}{M_2}\left(\frac{8}{M_1^2p_1^2}+\frac{8}{p_2^2}-\frac{16}{M_1p_1p_2}\right)+8\pi p\right]. \tag{52}$$

Adding the two parts of Eq. (47) yields

$$\begin{aligned}&2\pi+\frac{\pi\lambda z_3}{M_2}\left(\frac{8}{M_1^2p_1^2}+\frac{8}{p_2^2}-\frac{16}{M_1p_1p_2}\right)+8\pi p=2(h_1+h_2)\pi,\\ &\frac{\pi\lambda z_3}{M_2}\left(\frac{8}{M_1^2p_1^2}+\frac{8}{p_2^2}-\frac{16}{M_1p_1p_2}\right)+8\pi p=2h_3\pi,\end{aligned} \tag{53}$$

where h_3 is an integer. Since the initial phase of Eqs. (49) and (52) is an integral multiple of 2π when Eq. (47) is satisfied, the fringe amplitude of frequency $\left|\frac{2}{M_1M_2p_1}-\frac{2}{M_2p_2}\right|$ is enhanced. To subtract the two parts of formula (47), there exist

$$\begin{aligned}&\frac{\pi\lambda z_3}{M_2}\left(\frac{8}{M_1^2p_1^2}-\frac{8}{p_2^2}\right)+8\pi p=2(h_2-h_1)\pi,\\ &\frac{\pi\lambda z_3}{M_2}\left(\frac{8}{M_1^2p_1^2}-\frac{8}{p_2^2}\right)+8\pi p=2h_4\pi,\end{aligned} \tag{54}$$

where h_4 is an integer. From Eq. (54) we may see that when Eq. (47) is satisfied, the initial phase of Eqs. (50) and (51) is an integral multiple of 2π. Therefore, the fringe amplitude of frequency $\left|\frac{2}{M_1M_2p_1}-\frac{2}{M_2p_2}\right|$ is further strengthened.

Case 2 Dual $\pi/2$-phase grating interferometer.

Following an analysis process similar to the double π-phase grating, the optimal visibility conditions of dual $\pi/2$-phase grating interferometer may be expressed as

$$\begin{cases}\dfrac{\lambda z_3}{M_2}\left(\dfrac{1}{M_1^2p_1^2}-\dfrac{1}{M_1p_1p_2}\right)+p=\dfrac{2h_1+1}{2},\\ \dfrac{\lambda z_3}{M_2}\left(\dfrac{1}{p_2^2}-\dfrac{1}{M_1p_1p_2}\right)=\dfrac{2h_2+1}{2}.\end{cases} \tag{55}$$

3. Simulations and experiments

The simulations and experiments were performed with an x-ray tube (L9421-02, Hamamatsu Photonics K. K., Japan) with 5 μm focal spot (40 kVp, 200 μA). The pixel size of the flat panel detector (Shadobox 6K HS, Teledyne Dalsa, USA) was 50 μm with field of view of 14.7×11.52 cm^2. The two phase gratings with period of 3 μm were π-shift phase gratings at 28 keV, and they all had a duty cycle of 50%. The setup was arranged as follows: $z_1=1.2698$ m, $z_2=0.026$ m and $z_3=1.2698$ m. By the illumination of the polychromatic x-ray, the simulation fringe with period of 300 μm is shown in Fig. 2(a). Figure 2(c) presents the experimental result attained by the abovementioned simulation parameters. The period of the fringe perpendicular to the red line is 281.57 μm, which is

95% of the fringe period in Fig. 2(a). The error mainly comes from the measurement of the distance between different components.

In Figs. 2(a) and 2(c), the positions of the dual π-phase gratings are not nearby the positions where the fringe visibility is optimal. Therefore, the imaging period is twice as long as the theoretical result, such as the results given by Miao *et al.*[16] and Wang *et al.*[17] When the positions of the dual π-phase gratings are nearby the positions where the fringe visibility is optimal, e.g., $z_1 = 2.5395$ m, $z_2 = 0.0513$ m, $z_3 = 2.5395$ m, the fringe period in Fig. 2(b) is the same as that under monochromatic x-ray illumination. The experimental results given by Lei *et al.*[18] and Ge *et al.*[7] could well prove the above theory. Note that only the effect of the spectrum could not double the fringe period, and the positions of the phase gratings must also be considered. A similar situation is whether monochromatic or polychromatic x-ray is used, the period of self-imaging of a π-phase grating in the Talbot–Lau interferometer at the fractional Talbot order is $0.5Mp$, not Mp, where M is the system magnification and p is the period of the π-phase grating.

Surprisingly, the fringe shown in Fig. 2(c) has a two-dimensional structure, although the phase gratings used in the experiment are one-dimensional. In Fig. 2(c), the period of lattice structure perpendicular to the blue line is 722.34 μm, which is 2.57 times longer than the period of the fringe perpendicular to the red line. The lattice structure along the blue line is produced by the supporting structure of the phase gratings, denoted by the arrow in Fig. 2(d), and its period is 7.6 μm. The ratio of the period of the supporting structure to the period of the grating bar is 2.53:1, which is very close to the ratio of the fringe periods imaged by the two structures. Note that the dark area of the fringe is wider than the bright area of the fringe in Fig. 2(c). The reason is that the fringe visibility in Fig. 2(c) is very low (about 4% on average). In this situation, the low-intensity peaks in the fringe appear in black in the image, while the high-intensity peaks in the fringe appear in white.

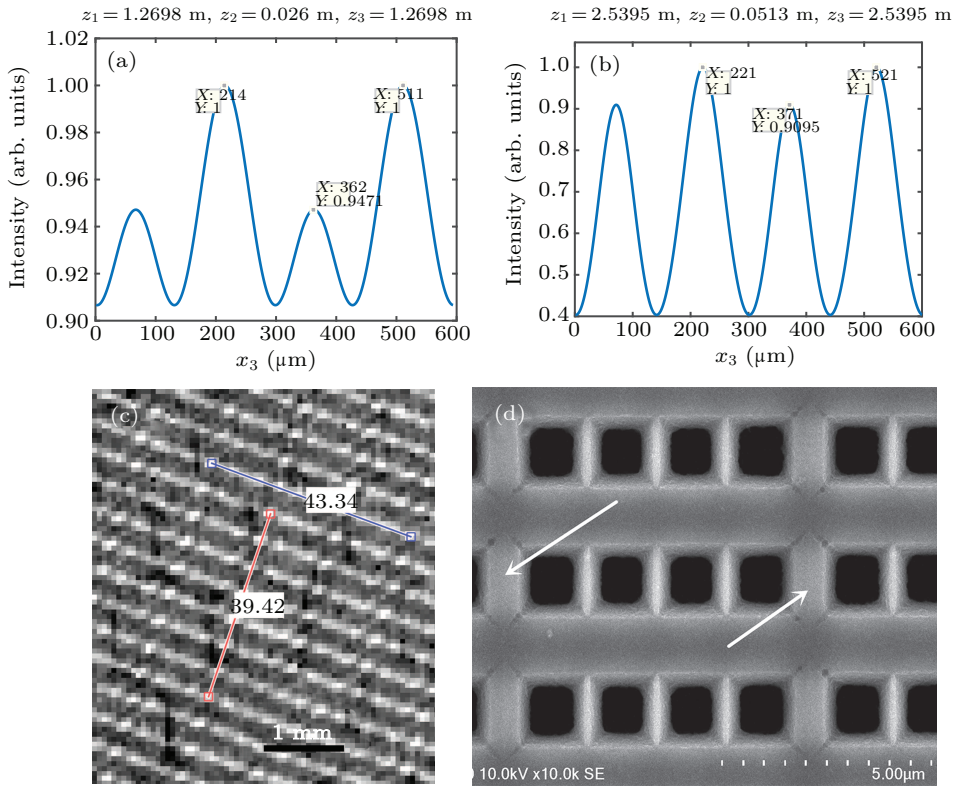


Fig. 2. (a) Simulation fringe obtained at $z_1 = 1.2698$ m, $z_2 = 0.026$ m and $z_3 = 1.2698$ m. (b) Simulation fringe obtained at $z_1 = 2.5395$ m, $z_2 = 0.0513$ m and $z_3 = 2.5395$ m. (c) Experimental result. The numbers beside the lines denote the number of pixels contained in the lines. (d) The SEM of the phase grating.

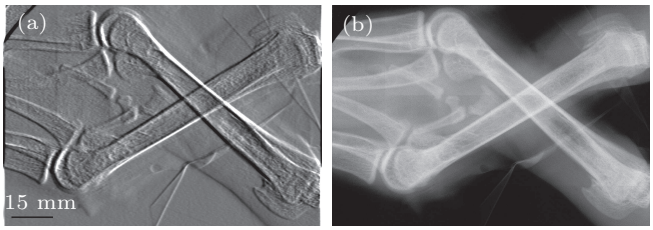


Fig. 3. (a) Differential phase image and (b) absorption image of the duck claws.

Two duck claws are imaged in the dual-phase grating interferometer. A phase-contrast image and an absorption image are retrieved by Fourier transform, as shown in Fig. 3. The distance between the duck claws and the detector is 100 cm. Ten images are acquired for noise reduction, and the acquisition time of each image is 15 s. The cartilage in the joint of the duck claws is clearly visible in the differential phase image,

and the effective field of view is 4.8×7 cm^2. By increasing the area of the phase grating, the field of view is further improved.

4. Conclusion

We have successfully obtained the fringe period and the optimal visibility conditions of the dual phase grating interferometer. The dual π-phase grating interferometer and the dual $\pi/2$-phase grating interferometer have different fringe periods and optimal visibility conditions. Under the illumination of polychromatic x-ray, the fringe period is twice as long as the theoretical result, when the positions of π-phase gratings are far away from the positions where the fringe visibility is optimal. The phase gratings used in this study are the two halves of a phase grating with a diameter of 5 inch.[20] If complete 8-inch phase gratings are used, the field of view can be further expanded to meet imaging requirement of human fingers.

Acknowledgements

This work was supported by the National Natural Science Foundation of China (Grant Nos. 11674232, 62075141, and 12075156) and the Foundation of Shenzhen Science and Technology Bureau, China (Grant No. 20200812122925001).

References

[1] Pfeiffer F, Weitkamp T, Bunk O and David C 2006 *Nat. Phys.* **2** 258
[2] Pfeiffer F, Bech M, Bunk O, Kraft P, Eikenberry E F, Bronnimann C, Grunzweig C and David C 2008 *Nat. Mater.* **7** 134
[3] Schleede S, Meinel F, Bech M, Herzen J, Achterhold K, Potdevin G, Malecki A, Adam-Neumair S, Thieme S, Bamberg F, Nikolaou K, Bohla A, Yildirim A, Loewen R, Gifford M, Ruth R, Eickelberg O, Reiser M and Pfeiffer F 2012 *Proc. Natl. Acad. Sci. USA* **109** 17880
[4] Bech M, Tapfer A, Velroyen A, Yaroshenko A, Pauwels B, Hostens J, Bruyndonckx P, Sasov A and Pfeiffer F 2013 *Sci. Rep.* **3** 3209
[5] Yang J, Zong F K, Lei Y H, Huang J H, Liu J Y and Guo J C 2019 *J. Phys. D: Appl. Phys.* **52** 195401
[6] Yoshioka1 H, Kadono Y, Kim Y T, Oda H, Maruyama T, Akiyama Y, Mimura T, Tanaka J, niitsu M, Hoshino Y, Kiyohara J, nishino S, Makifuchi C, Takahashi A, Shinden Y, Matsusaka N, Kido K and Momose A 2020 *Sci. Rep.* **10** 6561
[7] Ge Y S, Chen J W, Zhu P P, Yang J, Deng S W, Shi W, Zhang K, Guo J C, Zhang H T, Zheng H R and Liang D 2020 *Opt. Express* **28** 9786
[8] Zhu P P, Zhang K, Wang Z L, Liu Y J, Liu X S, Wu Z Y, McDonald S A, Marone F and Stampanoni M 2010 *Proc. Natl. Acad. Sci. USA* **107** 13576
[9] Wang Z L, Zhou R C, Zhao L M, Ren K, Xu W, Liu B and Chen H 2021 *Chin. Phys. B* **30** 028702
[10] Wang Z T, Hauser N, Singer G, Trippel M, Kubik-Huch R, Schneider C and Stampanoni M 2014 *Nat. Commun.* **5** 3797
[11] Yaroshenko A, Hellbach K, Yildirim A, Conlon T, Fernandez I, Bech M, Velroyen A, Meinel F, Auweter S, Reiser M, Eickelberg O and Pfeiffer F 2015 *Sci. Rep.* **5** 17492
[12] Scherer K, Yaroshenko A, Bolukbas D, Gromann L, Hellbach K, Meinel F, Braunagel M, Berg J, Eickelberg O, Reiser M, Pfeiffer F, Meiners S and Herzen J 2017 *Sci. Rep.* **7** 402
[13] Yang J, Guo J C, Lei Y H, Yi M H and Chen L 2017 *Chin. Phys. B* **26** 028701
[14] Momose A 2020 *Phys. Medica* **79** 93
[15] Donath T, Chabior M, Pfeiffer F, Bunk O, Reznikova E, Mohr J, Hempel E, Popescu S, Hoheisel M, Schuster M, Baumann J and David C 2009 *J. Appl. Phys.* **106** 054703
[16] Miao H X, Panna A, Gomella A, Bennett E, Znati S, Chen L and Han W 2016 *Nat. Phys.* **12** 830
[17] Kagias M, Wang Z T, Jefimovs K and Stampanoni M 2017 *Appl. Phys. Lett.* **110** 014105
[18] Lei Y H, Liu X, Huang J H, Du Y, Guo J C, Zhao Z G and Li J 2018 *J. Phys. D: Appl. Phys.* **51** 385302
[19] Yan A M, Wu X Z and Liu H 2018 *Opt. Express* **26** 23142
[20] Guo J C, Liu X, Zhou B, Du Y, Lei Y H and Niu H B 2012 *AIP Conf. Proc.* **1466** 61